J Solid State Electrochem (2012) 16:993–1001
DOI 10.1007/s10008-011-1475-8

ORIGINAL PAPER

Studies on electrodeposition of Zn–MoS_2 nanocomposite coatings on mild steel and its properties

Vathsala Kanagalasara · Thimmappa Venkatarangaiah Venkatesha

Received: 15 November 2010 / Revised: 10 June 2011 / Accepted: 13 June 2011 / Published online: 24 June 2011

Abstract Pure zinc and Zn–MoS_2 composite coatings were prepared by electrodeposition from zinc sulfate–chloride bath containing uniformly dispersed MoS_2 nanoparticles. The effect of MoS_2 on the deposition properties morphology, crystallographic orientation, and corrosion behavior were studied. The electrokinetic properties (zeta potential) and size distribution statistics in plating bath for the particles were evaluated using dynamic light scattering experiments. The Zn and Zn–MoS_2 deposition process was studied by linear polarization and cyclic voltammetry. Scanning electron microscopy, energy dispersive X-ray analysis, X-ray diffraction analysis, and potentiodynamic polarization measurements were used to characterize the coatings. The addition of MoS_2 to the electrolyte significantly changed the microstructure and crystallographic orientation of the zinc deposits and enhanced the corrosion resistance of the coatings. The morphological and electrochemical properties of the zinc coatings were observed to be significantly affected by the incorporation of MoS_2 particles into the zinc matrix.

Keywords Zeta potential · Composite coating · Electrodeposition · Zn–MoS_2 composite · Corrosion

V. Kanagalasara · T. V. Venkatesha (✉)
Department of Studies in Chemistry, School of Chemical Sciences, Kuvempu University,
Shankaraghatta 577451, Karnataka, India
e-mail: drtvvenkatesha@yahoo.co.uk

V. Kanagalasara
e-mail: vathsala.mahesh@gmail.com

Introduction

An insoluble, second-phase particle is suspended in a conventional plating electrolyte and is engulfed into the growing metal film. The technique has been widely demonstrated for a variety of metal-particle systems where the mean particle size is in nanometers to micron range. Electrodeposition offers a cost-effective process to fabricate such type of composite coatings onto the different-shaped metal surfaces [1–4].

Zinc coatings are widely used for the corrosion protection of ferrous materials, acting both as a physical barrier from the surrounding corrosive environment and as a self-sacrificial anodic protective layer. In the recent years, significant research efforts have focused on the electrodeposition of zinc coatings from various electrolytes into which different organic and inorganic compounds have been introduced to improve the deposit properties, morphology, and corrosion behavior [5–7].

MoS_2 is often dispersed in metal matrices like copper and nickel to achieve enhanced strength of the final composite material for good wear resistance [8–10]. Chang has prepared the nickel–MoS_2 composite by electrodeposition and examined its electrocatalytic properties in alkaline electrolytes. The effects of pH, current density, particle concentration, and temperature on the effectiveness of molybdenum disulfide incorporation in the nickel–MoS_2 composite have also been reported [11].

In the present study, Zn–MoS_2 composite coatings were prepared by electrodeposition from a sulfate–chloride-based bath containing dispersed MoS_2 nanoparticles. The effect of suspended MoS_2 on hydrogen evolution, polarization, and

corrosion resistance of the composite coatings was investigated. The microstructure and surface morphology were also analyzed.

Experimental

Plating experiments

A zinc sulfate plating bath composition used for the experiments is given in Table 1. The agglomeration of 40-nm-sized MoS_2 (Alfa Aesar, Ward Hill, MA, USA) was minimized by subjecting the electrolyte to magnetic stirring for a period of 12 h prior to plating experiments. The pH of bath solution was at 3.5, and it was adjusted by adding dilute H_2SO_4 or $NaHCO_3$.

Mild steel foils (AISI 1079 composition C=0.5%, Mn=0.5%, S=0.005%, and Fe=98.95%) with dimensions of 4×4×0.1 cm was used as cathode substrate. The mild steel was polished mechanically and degreased with trichloroethylene followed by water wash before subjecting to plating process. A Zn (99.9%) plate was used as the anode, and each time, its surface was activated by dipping in 10% HCl for few seconds, washed with water, and finally used for experiments. The anode and cathode of same dimensions were used for electrodeposition process. A potentiostat/galvanostat model PS-618 (Chemilink Systems, Mumbai) was used for the deposition of the coatings by DC currents. Electrodeposition experiments were performed under a constant current density of 4 A/dm^2, and the deposition time was 20 min. Throughout the deposition process, the electrolyte was stirred at a speed of 300 rpm.

Zeta potential and particle size measurements

Zeta potential (surface charge) of MoS_2 particles in plating bath was determined using a Zeta Plus™ zeta potential analyzer at 25 °C. The measured zeta potential is a reflection of the average mobility of the particles. The pH experiments were done by using the pH probe provided by Brookhaven Instruments Corp. with 90 Plus^{TM}. The particle size distribution of MoS_2 particles in plating bath was measured by dynamic laser light scattering analysis using a 90 Plus™ particle size analyzer (Brookhaven Instruments Corp., Holtsville, NY). Demonized water, obtained by processing of distilled water through Millipore purification (Milli-Q, USA) system, was used for the preparation of bath solutions.

Table 1 Composition of the plating bath

Components	Blank+MoS_2 (in g/L)	Zn+MoS_2 (in g/L)
$ZnSO_4{\cdot}7H_2O$	–	200
Na_2SO_4	30	30
NaCl	20	20
H_3BO_3	15	15
SDS (surfactant)	0.5	0.5
MoS_2	0–1	0–1

Coatings characterization

SEM and EDX measurements

The surface morphology of the coatings was investigated using JEOL-JEM-1200-EX II scanning electron microscope. The particle content in the film was determined by energy dispersive X-ray analysis (EDX) coupled with scanning electron microscopy (SEM). The EDX analysis was performed on the surface as well as on the cross section. The reported value of incorporated MoS_2 particles in the zinc matrix is an average value of three measurements.

XRD studies

X-ray diffraction (XRD)analysis of electrodeposits was carried out using a Philips TW 3710 X-ray diffractometer with Cu Kα radiation (λ=0.1540 nm), Ni filter working at 30 mA and 40 kV. The preferred orientation of the electrodeposits was estimated from the X-ray data. For the calculations, reference zinc ICDD-JCPDS card number 87-0713 and reference MoS_2 ICDD-JCPDS card number 39-1492 were used.

Electrochemical studies

Potentiodynamic polarization and electrochemical impedance spectroscopy measurements were performed using a CHI660C electrochemical work station. The measurements were performed using a conventional three-electrode cell, in which test sample was placed in Teflon sample holder and the exposed surface area to the corrosive medium was approximately 1 cm^2. The platinum wire serves as counter electrode and SCE electrode used as the reference electrode. Prior to the beginning of measurements, the sample was immersed in the corrosive medium (3.5% sodium chloride, pH neutral) in order to establish the open-circuit potential (E_{OCP}) or the steady state potential. The potentiodynamic polarization measurements were performed in non-deaerated conditions.

Deposition studies

The cathodic polarization profiles were recorded for both plating bath and blank solutions (without zinc ions) containing distinct amount of MoS_2 particles using mild

steel (0.13 cm^2 area) electrode at scan rate of 0.02 V/s. Prior to each experiment, the mild steel electrode was first polished with different grits of emery paper and then with alumina powders from 3 to 0.05 μm until to get mirror finish.

Tafel studies

The Tafel polarization study was used to calculate the kinetic parameters of the corrosion processes. The plots were obtained by varying the potential by ±200 mV from the open circuit potential at a scan rate of 0.01 V/s in 3.5% NaCl.

Results and discussion

Zeta potential and particle distribution

The ZetaPlus system has a laser beam which passes through the sample in a cell which carries two electrodes to provide the electric field. Thus, zeta potential analyzer measures both the direction and the velocity of the particles under the influence of a known electric field and then calculates mobility and zeta potential from this information. The relationship between zeta potential (ζ) and mobility depends on the theoretical model chosen. Here, we used the Smoluchowski limit for the calculations.

In principle, solid particles when come into aqueous interface tend to polarize and show electrical charge. If we apply an electric field to the liquid, then these charged particles will move towards either positive or the negative pole of the applied electric field. The direction they tend to move is a clear indication of the sign of the charge they carry. The velocity with which they translate is proportional to the magnitude of the charge. The nature and magnitude of the charge are the function of pH value. To know the adsorption of the charger species on particles, zeta potentials in solutions with different pH were measured and shown in Fig. 1. The zeta potential increases with decreasing pH. This may be due to the adsorption of H^+ ions on the surface of the particles [12].

Figure 2 shows the size distribution statistics for the MoS_2 particles in plating bath composition diluted to 100 times and stirred magnetically 12 h before use. This composite electrolyte was immediately used to measure the size distribution. The effective diameter of the particles may result from one or more populations of the particle distribution in electrolyte. This magnetically homogenized composite electrolyte resulted in a unimodel size distribution with different population of the particles. Here, it produces polydispersed colloidal system with polydispersity factor 0.2 (the factor less than 0.02 points the system is monodisperse). Also, the sample quality 3.8 (in the scale of 10 set by the manufacturer of the instrument) shows that the autocorrelation functions were calculated very well.

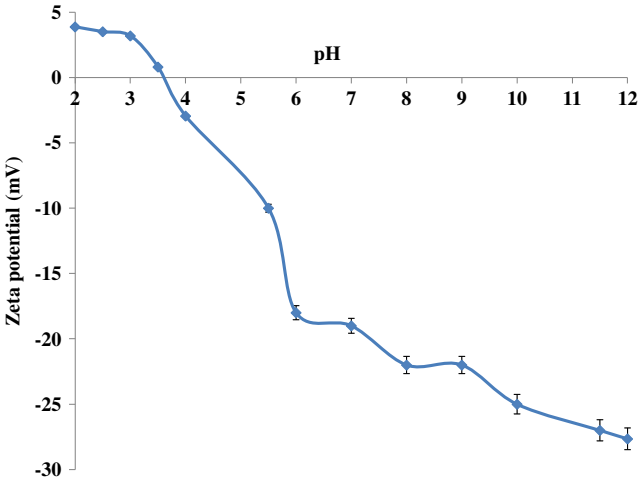

Fig. 1 Zeta potential of MoS_2 particles in aqueous solution measured at different pH

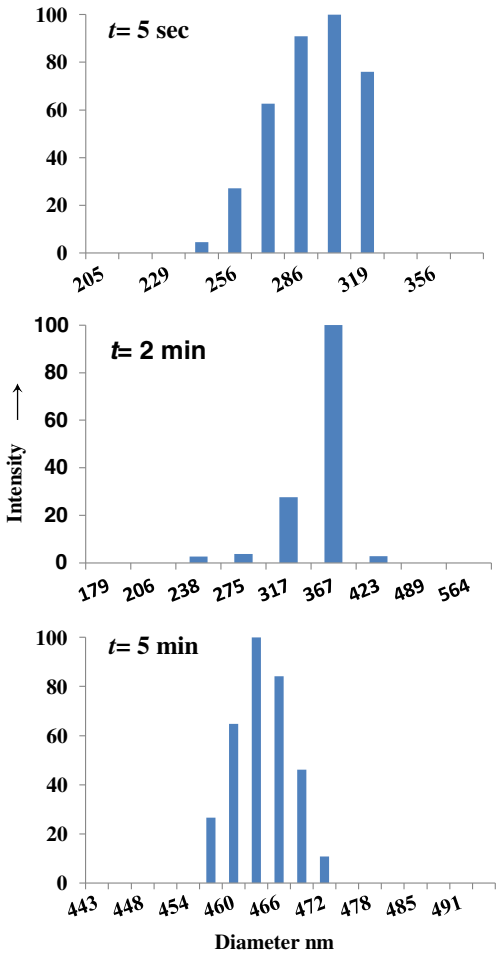

Fig. 2 Size distribution statistics graph of the MoS_2 particles dispersed in electroplating bath at pH 3.5 measured at different time intervals

As time increased, the effective diameter of the particles in solution also changed, i.e., at 5th second it was 295 nm, and after 2nd and 10th minutes, it agglomerated to 413 and 460 nm, respectively. This change in effective diameter is evidence for that plating solutions are thermodynamically unstable and kinetically stable; to maintain the bath stability and similar effective diameter of the MoS_2 particles, the deposition experiments were carried out at constant stirring conditions.

Polarization studies

To study the effect of MoS_2 particles on the reduction process during deposition process, cathodic polarization experiments were carried out. The cathodic polarization profiles were recorded for blank and zinc solutions with and without MoS_2 particles using mild steel (0.13 cm^2 area) electrode at scan rate of 0.01 V/s. Figure 3a–c shows cathodic sweeps on steel electrode in blank solution at different pH and at distinct concentration of MoS_2.

In Fig. 3a, it can be seen that a first limiting current density plateau related to the hydrogen evolution reaction (HER) from reaction (1) followed from that of the water reduction reaction (2).

$$H_3O^+ + 2e^- \rightarrow H_2 + OH^- \quad (1)$$

$$2H_2O + 2e^- \rightarrow H_2 + 2OH^- \quad (2)$$

The addition of MoS_2 to the blank solution at different pH cannot cause any new process, but their additions cause some kind of surface blockage on the electrode for the HER to occur. The adsorption of MoS_2 particles on the cathode suggests that the MoS_2 which were dispersed in the bulk solution are transported to electrode surface.

Many factors can have influence on this transportation of the MoS_2 particles on the cathode, maybe due to electrophoresis (positive surface chare), mechanical entrapment (by continuous stirring), adsorption (physically/weak forces), convection diffusion, etc. Many models have been reported in literature to explain this mechanism [13–15]. As the pH decreases, the zeta potential becomes more positive due to the increased adsorption of H^+ ions. This adsorption and surface blockage by codeposition mechanism are schematically represented in Fig. 4.

Figure 3b surmises that as the concentration of MoS_2 particles increases in the plating bath, the reduction current decreased due the more number of active sites in the cathode that are blocked by the MoS_2 particles, quenching the hydrogen evolution reaction. For the same potential values, smaller current densities were measured compared to the electrolyte which was free from MoS_2 at all three different pH. This effect is a function of concentration of MoS_2. This result indicates that in the conditions of the blank solution, MoS_2 particles were probably adsorbed onto the steel electrode minimizing the active surface area of it.

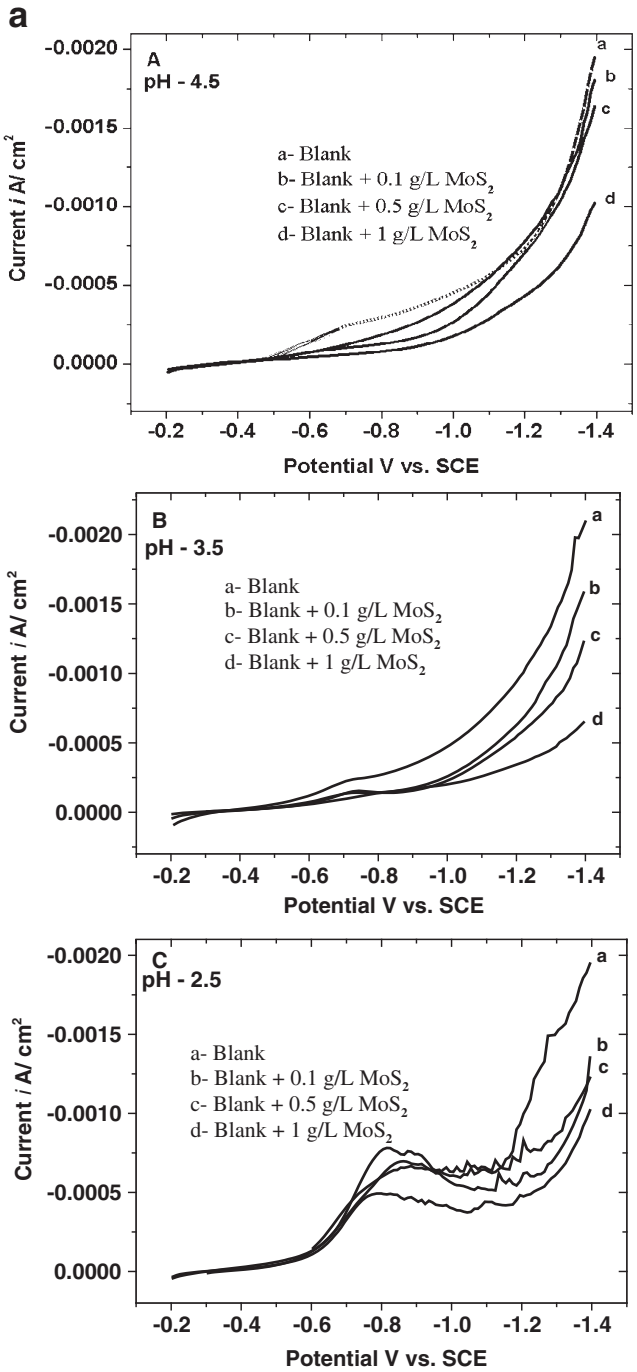

Fig. 3 **a** Cathodic polarization on steel electrode curves for the Blank solution (plating bath without zinc) at different pH *a* 4.5, *b* 3.5, and *c* 2.5, containing different amounts of MoS_2. **b** Effect of particle concentration on reduction current at different pH on steel electrode for blank solution (plating bath without zinc) at −1.25 V vs. SCE

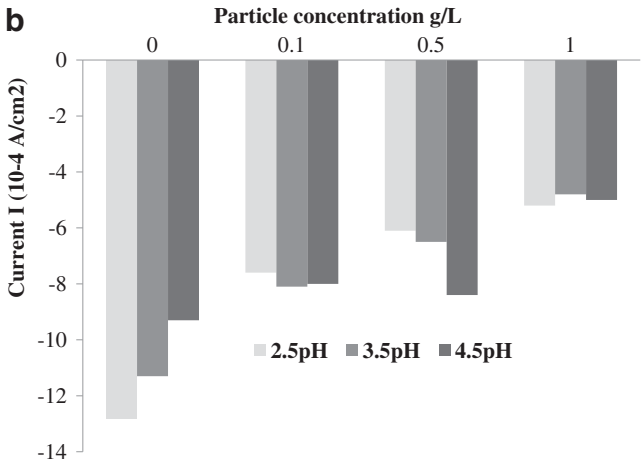

Fig. 3 (continued)

The cathodic polarization behavior of the Zn–MoS_2 electrolyte containing different concentration of MoS_2 particles at pH 3.5 is shown in Fig. 5. The curve "a" represents the polarization of mild steel electrode for pure zinc deposition from the bath solution without MoS_2 particles. The curves "b", "c," and "d" represent the polarization of steel electrode for Zn–MoS_2 composite coating from the bath solution containing 0.1, 0.5, and 1 g/L uniformly dispersed MoS_2 particles, respectively.

It is seen that the presence of MoS_2 particles shifts the reduction potential of Zn^{2+} ions to higher negative potentials when compared to reduction potentials of pure zinc deposition. Further, the potential shift was appreciable in solution containing 1 g/L of MoS_2.The result indicates that the MoS_2 particles in the electrolyte cause an increase in the cathodic polarization, but the slope is unchanged. This means that the adsorption of MoS_2 particles on cathode surface hinders the deposition of Zn^{2+} but does not significantly affect the electrochemical reaction mechanism.

The physical dispersion and electrophoretic migration of the particles in the electrolyte facilitate incorporation of particles into Zn metallic matrix. At higher concentrations of MoS_2, the polarization values were very similar to the bath solution containing 1 g/L MoS_2 particles which may be due to the aggregation of MoS_2 particles at the bottom of the cell during electrodeposition, making the effective concentration of MoS_2 smaller. Therefore, the concentration of MoS_2 in the bath solution was limited to 1 g/L.

Figure 6 shows the effect of different concentration of MoS_2 on zinc electrodeposition using cyclic voltammetry at pH 3.5 for bath solution, containing different amounts of MoS_2. The cyclic voltammetric experiments were initiated at −0.4 V in a negative direction and reversed at −1.4 V in a positive direction to −0.4 V at a scan rate of 0.01 V/s. The reduction peaks I_c is clearly associated with the massive reduction of Zn^{2+} to Zn. When the sweep was reversed, an oxidation peak I_a was observed due to the oxidation of the deposit.

The reduction of zinc begins at −1.135 V vs. SCE for pure zinc, and −1.139, −1.153, and −1.163 V vs. SCE for electrolyte containing 0.1, 0.5, and 1 g/L MoS_2, respectively. When the MoS_2 concentration was 0.1 g/L, the electroreduction peak partially was unaffected, but the electro-oxidation of deposit showed a decrease of I_a. For the higher MoS_2 concentration, the reduction shifted slightly towards more negative potentials and the peak reduction current (I_c) decreases slightly. Simultaneously, the electro-oxidation peak current density (I_a) decreased as the concentration of MoS_2 was increased. This could be attributed to the surface blockage of the electrode by MoS_2 particles. Decreased anodic dissolution rate may be due to the extra chemical stability possessed composite by the inclusion of MoS_2 into the deposit. When the direction of potential sweep is reversed, a cross-over potential associated with nucleation is observed at −1.060 V vs. SCE. The cross-over potential remains same for both the zinc and composite electrolytes indicating no additional process during zinc nucleation.

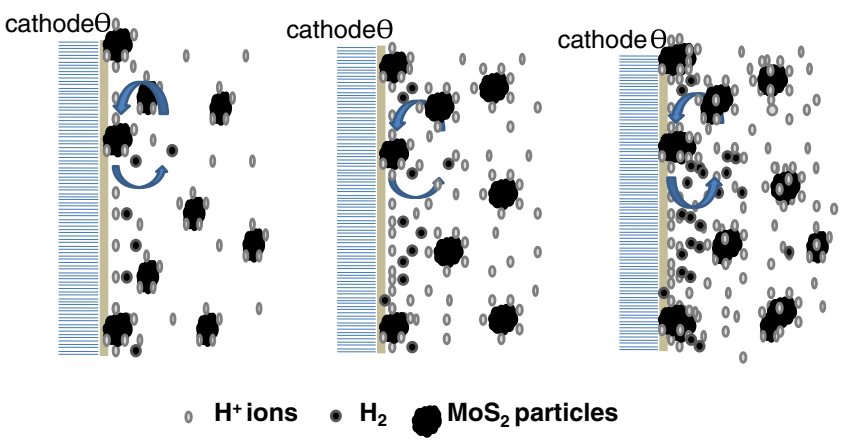

Fig. 4 The pictographic view of the H^+ adsorption on MoS_2 particles and HER reactions. The regions include different concentration of H^+ (decreasing pH), transportation, and codeposition of MoS_2 particles on the cathode surface

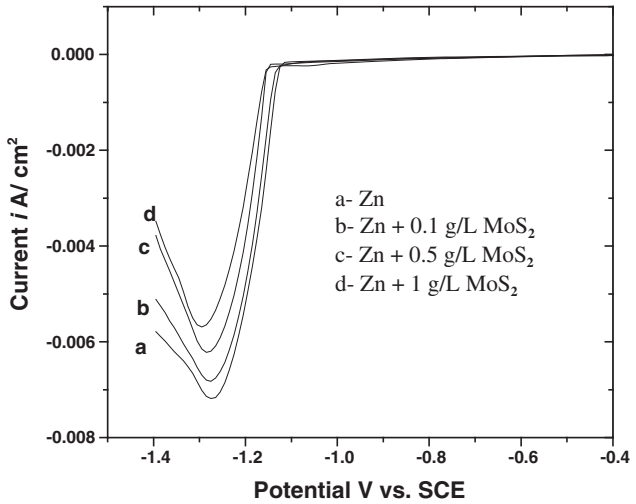

Fig. 5 Cathodic polarization curves for the deposition of Zinc and Zn–MoS_2 from the plating bath

The deposition studies illustrate that MoS_2 particles cause an obstructive effect on the Zn^{2+} reduction. In the literature, it is reported that the metal Me^{2+} electrodeposition takes place in several steps. It is accepted that an intermediate Me^{+} adsorption on the electrode during cathodic reaction [16, 17]. During electroreduction, the localized concentration of hydroxide ions in close proximity to the cathode surface will increase and result in the formation of $MeOH_{ads}$. The probable chemical reaction path of zinc ions reduction is specified below [18].

$$Zn^{2+}+H_2O \rightarrow (ZnOH)^{+}+H^{+} \tag{3}$$

$$(ZnOH)^{2+} + e^{-} \rightarrow Zn(OH)_{ads} \tag{4}$$

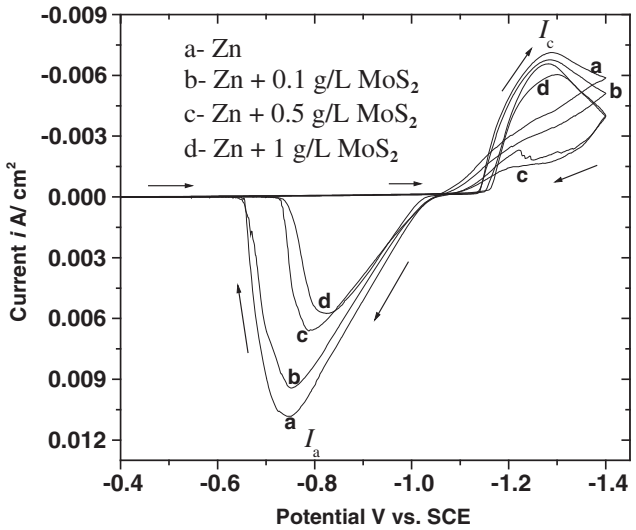

Fig. 6 Cyclic voltammetric curves for the Zinc and Zn–MoS_2 plating baths

$$Zn(OH)_{ads} + e^{-} \rightarrow Zn + OH^{-} \tag{5}$$

$$Zn(OH)_{ads} + (ZnOH)^{+} + 2e^{-} \rightarrow Zn + OH^{-} + Zn(OH)_{ads} \tag{6}$$

According to the cathodic polarization results, it is established that MoS_2 particles just block some active sites at the cathode/electrolyte interfaces. It also suggests that zinc ions are faintly adsorbed on the MoS_2 particles, as they are predominant as freely solvated ionic state in plating bath. So, there is a very less opportunity to subsequent intermediate $MoS_2{\cdot}Zn(OH)_{ads}$ catalytic reduction pathway. In addition, electrokinetic studies at different pH confirm that the adsorption of H^{+} on MoS_2 particles surface and possibility of following reactions are projected during electroreduction.

$$MoS_2 \cdot H^{+} + e^{-} \rightarrow MoS_2 \cdot H_{ads} \tag{7}$$

$$MoS_2 \cdot H_{ads} + H^{+} + e^{-} \rightarrow MoS_2 + H_2 \tag{8}$$

Surface morphology

Figure 7a, b shows the SEM images of zinc and Zn–MoS_2 (1 g/L) coated samples, respectively. The grain size of the composite coated sample was almost uniform, and it was smaller than zinc. These images indicate that the MoS_2 were distributed uniformly throughout coating and thereby provided more number of nucleation sites and retarded the crystal growth resulting in the formation of uniform grain size. The EDX analysis on the surface of composite coating confirmed the inclusion of about 1.4% of the MoS_2 into the zinc matrix.

XRD studies

The XRD patterns of the coatings were recorded using an X-ray diffractometer with Cu $K\alpha$ as the radiation source and Ni as the filter to identify the phases. The preferred orientation of the zinc electrodeposits was estimated from the X-ray data [19], where the texture coefficient (T_c) is calculated by using the equation below:

$$T_c = \frac{I_{(hkl)}}{\sum I_{(hkl)}} \times \frac{\sum I_{0(hkl)}}{I_{0(hkl)}} \tag{9}$$

where $I_{(hkl)}$ is the diffraction line intensity of the (hkl) reflection of zinc electrodeposits and $\Sigma I_{(hkl)}$ is the sum of the intensities of all the diffraction lines monitored. The I_0 refers to intensity of the reference zinc powder sample. For the calculations, reference zinc JCPDS card number 87-

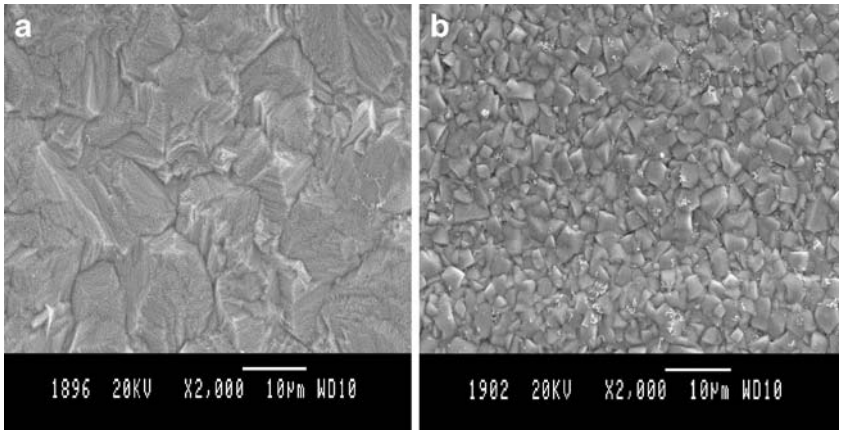

Fig. 7 SEM image of **a** zinc and **b** Zn–MoS_2 (1 g/L) coating

0713 was used. The size of the crystallites was obtained by using the Scherrer equation [20].

$$D = \frac{K\lambda}{B\cos\theta} \tag{10}$$

where D is the diameter of the crystal particle, K the shape factor (the typical value is 0.9), λ the wavelength of the incident beam, B the broadening of diffraction line measured in radians at half of its maximum intensity, and θ the Bragg angle.

The XRD pattern of the zinc and Zn–MoS_2 coatings prepared from the solution with and without 1 g/L MoS_2 particles are presented in Fig. 8a, using about 23-μm-thick coatings. XRD studies inferred that the average crystal size of composite sample is 21 nm against 26 nm of the zinc coating. The calculated texture coefficients are plotted in Fig. 8b. The analysis of the diffractogram indicates that the codeposition of MoS_2 into the zinc matrix has an influence on the orientation of the deposits. The majority of the lines can be ascribed to the zinc hexagonal structure.

The preferential crystal orientation of zinc electrodeposits depends on the experimental conditions such as current density, pH, temperature, and composition of the bath. The plane (002) has been associated with the hexagonal zinc crystal parallel to the substrate. In the absence of MoS_2, peaks associated with the characteristic crystallographic planes for zinc were observed. The peak associated with plane (002) having the highest intensity and texture coefficient. When the deposit was produced in the presence 1 g/L of MoS_2, a substantial decrease of (002) peak was observed, as well as the peaks associated with (104) and (101) changed by the incorporation of MoS_2.

The persistence of all those peaks, although with the less intensity, suggests the appearance of a zinc-rich η phase in composite coating. Since the diffraction pattern of Zn–MoS_2 coating η phase is very similar to zinc diffraction pattern. In the composite, the peaks associated with the planes (002), (101), (110), and (112) shifted from 36.61°, 43.53°, 70.34°,

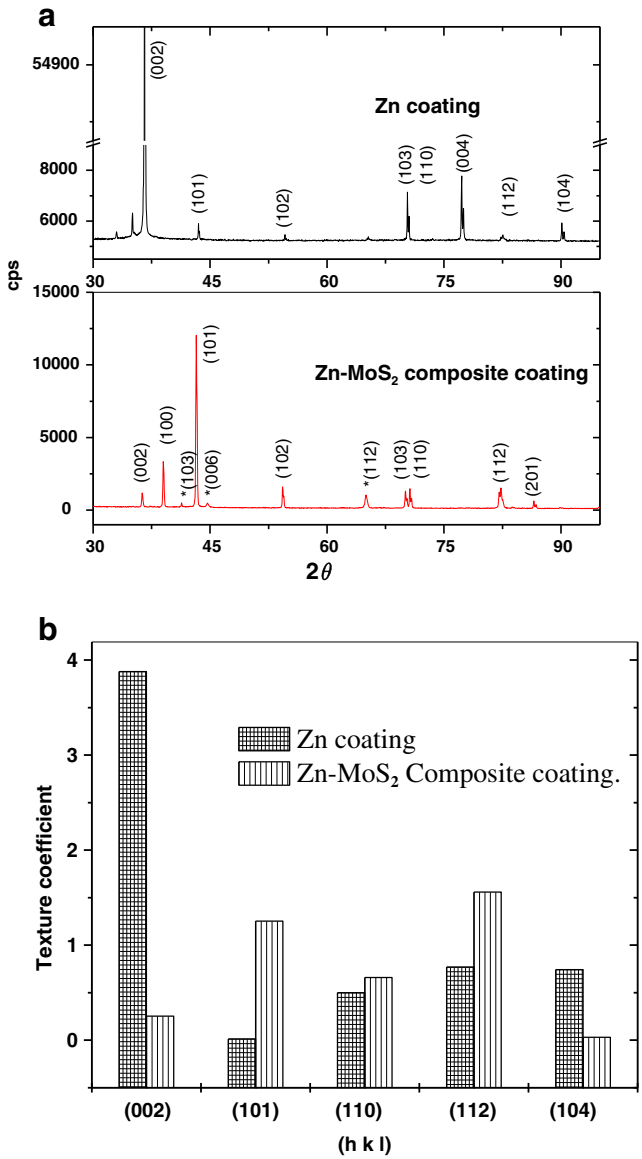

Fig. 8 **a** XRD patterns of zinc and composite coatings. **b** Preferential orientation for Zinc and Zn–MoS_2 (1 g/L) composite coatings

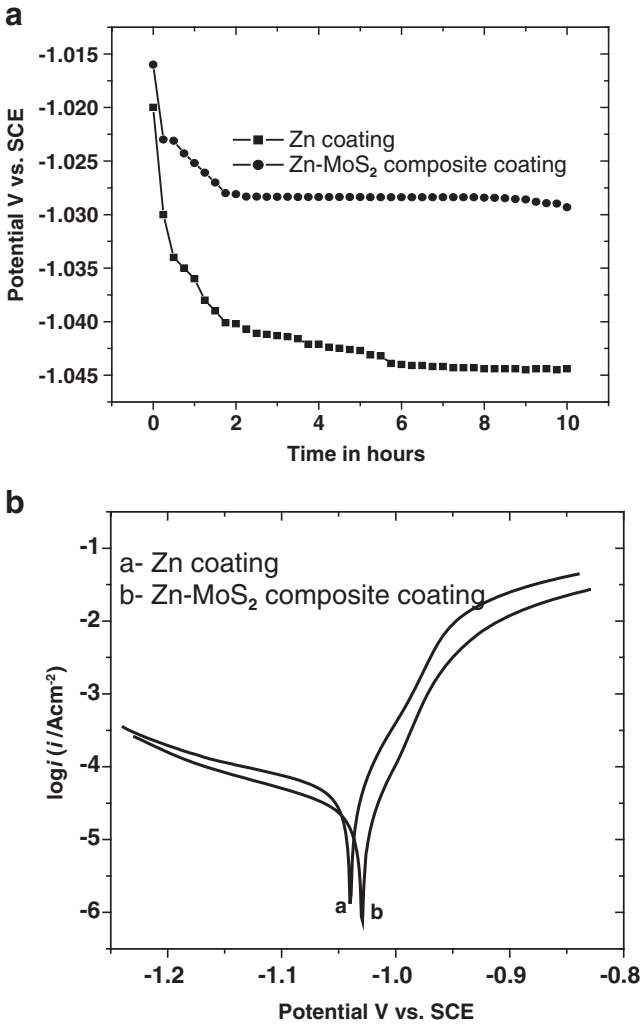

Fig. 9 **a** Variation of the OCP with the immersion time in 3.5% NaCl solution for the Zinc and Zn–MoS_2 (1 g/L) coatings. **b** Tafel curves of Zinc and Zn–MoS_2 (1 g/L) coatings in 3.5% NaCl solution

and 82.51° to 36.31°, 43.25° 70.43°, and 82.62°, respectively, indicating that the crystal lattice of the composite was deformed.

It can be seen that for the sample prepared in presence of 1 g/L MoS_2 solution, the majority of the crystallites are oriented parallel to the (112) and (101) planes, while the preferential crystallographic orientation of the zinc deposit is (002). This change in crystallographic orientations in zinc crystals may be due to MoS_2 adsorption on the zinc active sites and thus influences the growth rates of the zinc crystalline planes. This change in the X-ray pattern for the composite corresponds to the change in the electrochemical behavior seen in Fig. 3 and to the morphology observed in Fig. 7 may be associated with inclusion of MoS_2 in the deposit.

Corrosion studies

The composite coatings were obtained on mild steel samples from the bath solution containing 1 g/L of MoS_2, and also, the zinc deposit was produced without MoS_2 particles. The coatings were subjected to open-circuit potential (OCP) and Tafel experiments in 3.5% NaCl.

When a metallic species is immersed in the corrosive medium, both oxidation and reduction processes occur on its surface. The specimen assumes a potential relative to reference electrode. After attaining the equilibrium condition, both anodic and cathodic reaction rates are equal and there is no net current in the system, and this equilibrium potential is referred as OCP. If the system is disturbed from this equilibrium condition by polarization, the net current flows in the system and can be measured.

The variation of OCP with time for the zinc and Zn–MoS_2 (1 g/L) in 3.5% NaCl is shown in Fig. 9a, where both the coatings reached equilibrium within 2 h. Initially, the OCP was −1.020 and −1.016 V vs. SCE for zinc and composite, respectively. After 2 h, the coatings attain equilibrium potential. At equilibrium, zinc and composite coatings have −1.04 and −1.03 V vs. SCE, respectively. At any given time, the composite showed less negative potential for entire 10-h time duration compared to pure zinc coating. This implies that the composite coating acquired nobler character than zinc. This hinders anodic reaction, and hence, it tends to possess anticorrosion property.

Figure 9b shows the Tafel plots of zinc and Zn–MoS_2 (1 g/L) composite coatings. Corrosion characteristics such as corrosion potentials E_{corr}, corrosion rate (CR), and anodic cathodic slopes (β_a and β_c) were obtained from these results using the following Stern–Geary relationships [21].

$$I_{corr} = b/R_p \tag{11}$$

where b is constant value calculated by following equation:

$$b = \frac{\beta_a \cdot \beta_c}{2.3(\beta_a + \beta_c)} \tag{12}$$

$$CR(mpy) = 0.13\, I_{corr}(eq\ wt)/d \tag{13}$$

where eq wt is the equivalent weight and d is density in grams per cubic centimeter of zinc. The results of the

Table 2 Electrochemical parameters of the coatings derived from Tafel plots

Medium	Specimen	I_{corr} (A/cm^2)	E_{corr} (V)	β_c	β_a	CR (mil/year)
3.5% NaCl	Zinc	6.45×10^{-5}	−1.04	3.52	17.9	3.7×10^{1}
	Zn-MoS_2	3.78×10^{-5}	−1.03	4.31	14.98	2.2×10^{1}

potentiodynamic corrosion tests are tabulated in Table 2. The results indicate that the corrosion potential of Zn–MoS_2 composite coating is more positive and I_{corr} is also lower than that of zinc, which may be due to the incorporation of chemically inert MoS_2 particles in the zinc matrix. The values of the anodic and cathodic Tafel coefficients for composite coatings were different from that of pure zinc coating. This suggested that the presence of MoS_2 nanoparticles in zinc coating influences the kinetics of both the anodic and cathodic electrochemical reactions. The data clearly reveal that the composite coating posses better stability to the external environment than pure zinc coating. The MoS_2 act as inert physical barriers to the initiation and development of defect corrosion by modifying the microstructure of the zinc layer and hence helps to improve the corrosion resistance of the composite coating.

The corrosion resistance of Zn–MoS_2 composite coatings can be attributed to subsequent rationale. First, the MoS_2 particles have a low level of electronic conductivity and are dispersed in matrix so it can distract the corrosion current and results in the decrease of corrosion rate. Second, the MoS_2 particles are chemically inert that cannot be affected by corrosive medium, and the composite is compact. So, they could isolate the coating by decreasing the exposed area of the matrix from the corrosive medium and, as a result, restrain the corrosion process.

Conclusions

Zn–MoS_2 coatings were fabricated by using electrodeposition technique, and the coatings were characterized by EDX, polarization, SEM, and Tafel analysis. Based on the results of the above investigations pertaining to the production of Zn–MoS_2 coatings using sulfate–chloride zinc electrolyte the following conclusion can be drawn.

- The codeposition of MoS_2 particles with Zn^{2+} ions shifted the deposition potential of the zinc to more negative potential. The adsorption of the MoS_2 particles on the active cathode surface leads to the blockage of the active surface area and which offers a polarization to reduction process.
- The addition of MoS_2 to the electrolyte significantly altered the morphology and changed the preferred orientation of the zinc basal planes of the deposits.
- Incorporated MoS_2 enhanced the corrosion resistance of the zinc composite compared to the zinc coating.

Acknowledgments The authors are grateful to Kuvempu University Shankaraghatta, Karnataka for providing lab facilities. The authors are grateful to the Department of Science and Technology [DST: project sanction no.100/IFD/1924/2008-2009 dated February 07, 2008], New Delhi, Government of India for providing financial assistance.

References

1. Kalendova A (2003) Prog Org Coat 46:324–332
2. Low CTJ, Wills RGA, Walsh FC (2006) Surf Coat Technol 201:371–383
3. Meenu S, William Grips VK, Rajam KS (2008) Mater Lett 62:3487–3489
4. Huang ZJ, Xiong DS (2008) Surf Coat Technol 202:3208–3214
5. Xia X, Zhitomirsky I, McDermid JR (2009) J Mat Proces Technol 209:2632–2640
6. Ilieva M, Ivanov S, Tsakova V (2008) J App Electrochem 38:63–69
7. Zheng H, Maozhong AN, Junfeng LU (2006) Rare Metals 25:174–178
8. Fox VC, Renevier N, Teer DG, Hampshire J, Rigato V (1999) Surf Coat Technol 116–119:492–497
9. Renevier NM, Oosterling H, Konig U, Dautzenberg H, Kim BJ, Geppert L, Koopmans FGM, Leopold J (2003) Surf Coat Technol 172:13–23
10. Jeffrey RL, Hyun IK, Paul MA, Daniel JD, Michael TD (2009) Thin Solid Films 517:5516–5522
11. Yu CC, Ying YC, Chun IL (1998) Electrochim Acta 43:315–324
12. Gang W, Ning L, Dian Long W, De Rui Z, Bo Qing X, Kurachi M (2004) Mater Chem Phys 87:411–419
13. Guglielmi N (1972) J Electrochem Soc 119:1009–1011
14. Celis J, Roos J, Buelens C (1987) J Electrochem Soc 134:1402–1408
15. Fransaer J, Celis J, Roos J (1992) J Electrochem Soc 139:413–418
16. Cachet C, Wiart R (1994) J Electrochem Soc 141:131–140
17. Cachet C, Wiart R (1999) Electrochim Acta 44:4743–4751
18. Yan H, Downes J, Boden PJ, Harris SJ (1996) J Electrochem Soc 143:1577–1583
19. Fustes J, Gomes A, da Silva Pereira MI (2008) J Solid State Electrochem 121:1435–1443
20. Scherrer P (1918) Math Phys 2:98–100
21. Stern M, Geary AL (1957) J Electrochem Soc 104:56–63